MODELING THE TEMPERATURE-DEPENDENT STRUCTURAL PERFORMANCE OF RIGID POLYURETHANE AND POLYISOCYANURATE FOAMS USING MEAN-FIELD HOMOGENIZATION AND FINITE ELEMENT ANALYSIS

Hieu T. McElroy[(1)] and Luca Guj[(2)]
The Dow Chemical Company
[(1)]Lake Jackson, TX, United States
[(2)]Horgen, Switzerland

ABSTRACT

In recent years, rigid Polyurethane (PUR) and Polyisocyanurate (PIR) foams are increasingly used as insulation materials for wall and roof applications in high energy-efficient homes and commercial buildings around the world due to their superior thermal performance. Metal-faced PUR/PIR sandwich panels are widely used as structural insulated panels in commercial building applications to reduce construction time as well as materials and costs associated with structural framing. Thus, material manufacturers must understand the structural performance of PUR/PIR foams to ensure the foam panels meet the quality requirements and industry standards. Because manufacturing and characterization are expensive, time-consuming, and labor-intensive, Dow Research and Development (R&D) has developed a combined experimental-numerical approach to model the anisotropic temperature-dependent properties of rigid PUR/PIR foams. This approach allows predictions of thermal-mechanical properties, i.e., tensile and compression behaviors, to end-use performance, e.g., metal-faced sandwich solutions for commercial buildings. The numerical model is based on the "double-inclusion" mean-field homogenization technique and finite element analysis. Finally, the model was experimentally validated using tensile and four-point bending tests as well as digital image correlation analysis.

Corresponding author: Hieu T. McElroy (htruong@dow.com)

1. INTRODUCTION

Rigid Polyurethane (PUR) foam panels have been used for insulation in the construction industry for a few decades. With recent technical advancements, the next-generation rigid foam products, so-called Polyisocyanurate (PIR) foams, were developed. PIR foams have superior performance regarding processability, weight reduction, structural strength, adhesion to metal facings, thermal insulation and, fire performance. Therefore, PIR foams have gained shares in different market segments, e.g., metal-faced sandwich solutions for commercial and institutional buildings and pipe-in-pipe for oil and gas applications. In recent years, metal-faced PIR sandwich panels have been widely used as structural insulated panels in energy-efficient homes and commercial building applications around the world to reduce construction time as well as materials and costs associated with structural framing.

Copyright 2020 by the Dow Chemical Company. Published by the Society of the Advancement of Material and Process Engineering with permission.

SAMPE Virtual Conference Proceedings, 2020. Society for the Advancement of Material and Process Engineering – North America.

It is essential to understand the structural performance of PUR/PIR foams to ensure the foam panels meet the quality requirements and industry standards [1]. Manufacturing and characterization are often expensive, time-consuming, and labor-intensive. Thus, Dow Research and Development (R&D) has developed a combined experimental-numerical approach to model the anisotropic temperature-dependent properties of rigid PUR/PIR foams. This approach allows predictions of thermal-mechanical properties, i.e., tensile and compression behaviors, to end-use performance, e.g., metal-faced sandwich solutions for commercial buildings. The numerical model is based on the "double-inclusion" mean-field homogenization (MFH) technique and finite element analysis (FEA). Finally, the model was experimentally validated using tensile and four-point bending tests as well as digital image correlation (DIC) analysis.

2. BACKGROUND: FUNDAMENTALS OF RIGID FOAM PANELS' PROCESSING AND CHARACTERISTICS

Rigid PUR/PIR foams are made by mixing and chemical reactions of a number of components: polyol, isocyanate, blowing agent, catalysts, surfactants, and other additives. The result is a closed-cell foam structure containing PUR/PIR cell walls enclosing a combination of gas (the majority is CO_2). Figure 1 illustrates the components and products of the reaction.

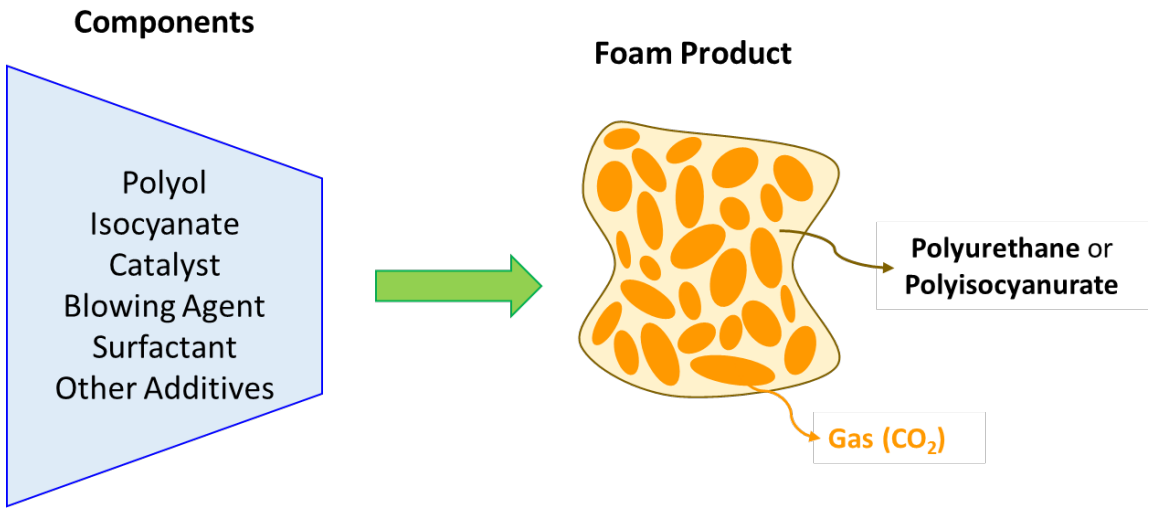


Figure 1. Components and products of PUR/PIR foams.

Metal-faced PUR/PIR sandwich panels are made using the Rigid-Faced Double Belt Lamination (RFDBL) process, demonstrated in Figure 2(a). The process consists of mixing the components described previously to obtain a reacting mixture. This mixture is then uniformly distributed on the bottom metal sheet across the panel width using a distributor, often referred to as poker, while both the top and bottom metal sheets are continuously pulled along the advance (length) direction. The physicochemical blowing process occurs, leading to the formation of foam, and as the foam rises up, the gap between the two moving metal sheets is filled. Finally, panels of the desired length are cut out. An example of the final product is shown in Figure 2(b).

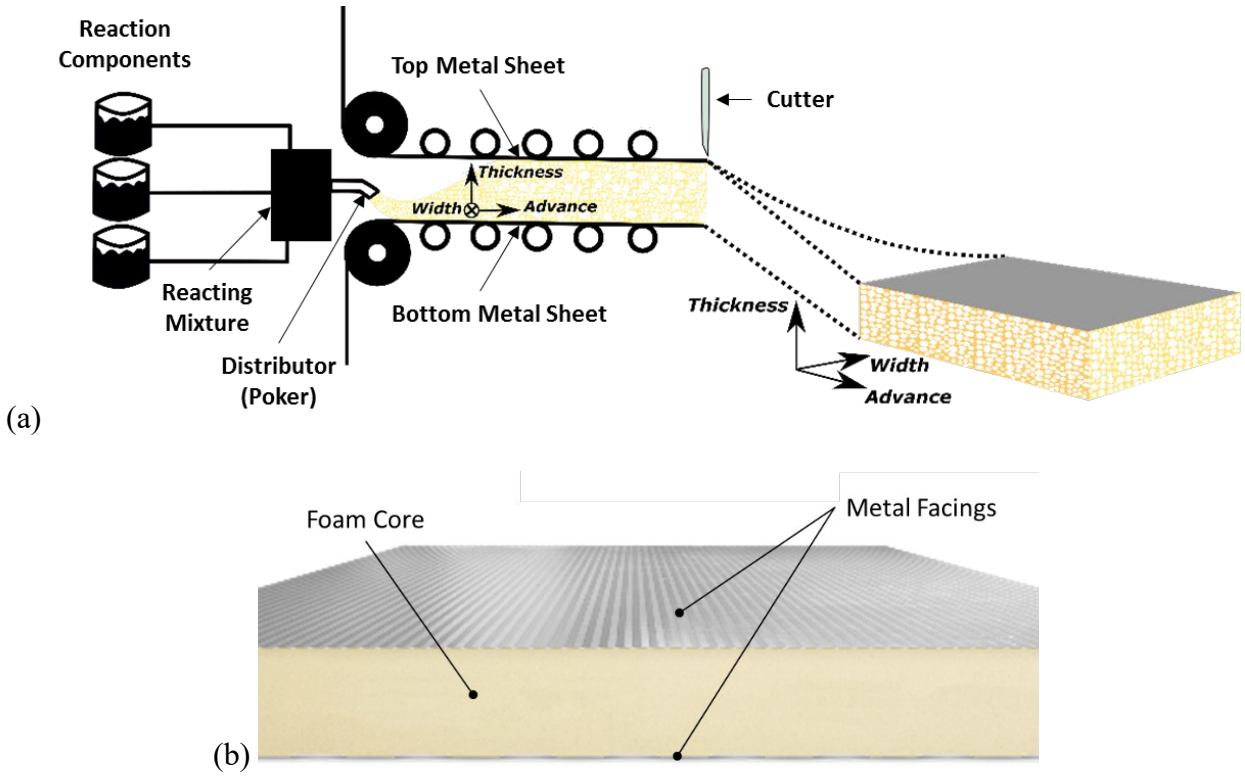


Figure 2. (a) PUR/PIR foams' directions related to the RFDBL production process (b) Typical insulated metal panel for constructions.

As a result of the manufacturing process, the foam cells are elongated and oriented along the advance direction. In addition, the foam microstructure (cell size and foam density) varies through the panel's thickness, i.e., the density decreases, and cell size increases from the bottom to the top of the panel. Nevertheless, the foam microstructure is relatively uniform across the panel's width. The advance, width, thickness directions in the metal foam panels are illustrated in Figure 2(a). The variations in the foam microstructure lead to anisotropic thermal-mechanical behaviors. Generally, PUR/PIR rigid foams are brittle and exhibit relatively linear-elastic behavior in tensile loadings. An example of the anisotropic stress-strain response of PIR foam in tension at room temperature is shown in Figure 3(a). Because the foam cells are oriented in the advance direction, the tensile modulus of samples tested in the advance direction is significantly higher than the tensile modulus of samples tested in the width and thickness directions. In the width and thickness directions, the foam has similar stiffness and strains at failure. For simplicity of modeling and analysis, in this work, it is assumed that the rigid foams exhibit transversely isotropic behavior in the width and thickness (W&T) directions, exemplified by the average tensile behavior among the two directions, i.e., W&T behavior in Figure 3(a). The schematic of rigid foams' transversely isotropic microstructure is shown in Figure 3(b).

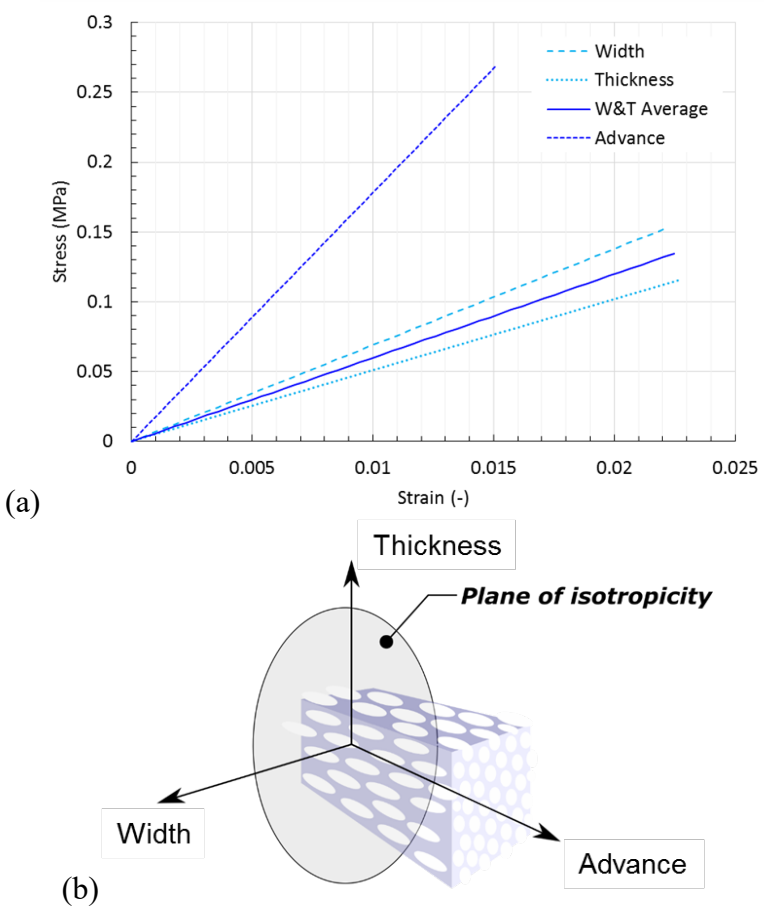


Figure 3. (a) Anisotropic behavior of a PIR foam in tension at room temperature (b) Schematic of rigid foams' transversely isotropic microstructure.

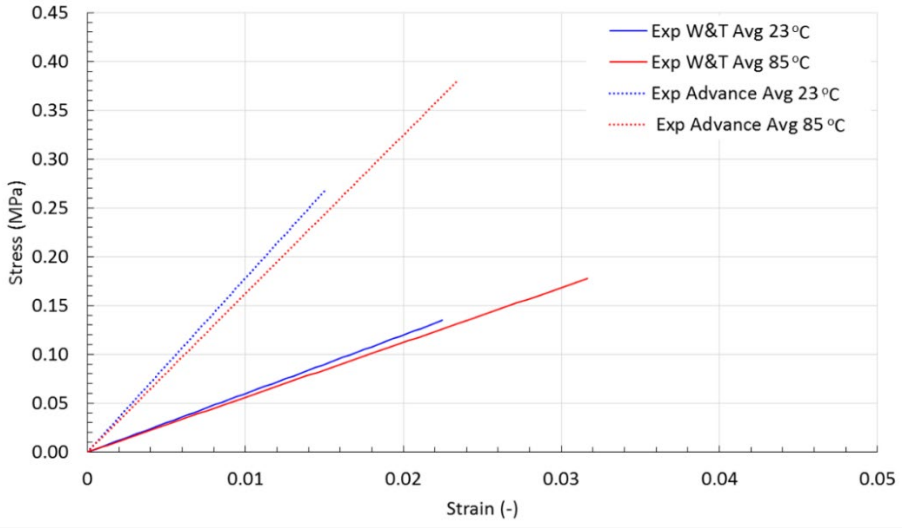


Figure 4: Tensile behavior: Advance vs. W&T direction at 23°C and 85°C.

At high temperatures, the foams still exhibit relatively linear-elastic and transversely isotropic behavior. The moduli are, however, decreased while the values of strain at break increase. Figure 4 shows the comparison of tensile stress-strain responses obtained at 23 ºC and 85 ºC of a PIR foam.

3. MODELING

3.1 Mean-Field Homogenization Approach

The constitutive model proposed by Dow R&D was designed to represent the structural behavior of PUR/PIR rigid foams within different end-applications. The structural performance of PUR/PIR foams is measured not only in terms of stiffness but also in terms of strength. During service, metal-faced rigid foam panels experience failures induced by thermal cycles. These thermal cycles are caused by either weather conditions (i.e., solar radiation and rain wash) or the after-production cooling cycles, especially when the operating temperature is well below freezing. The proposed model can depict all of the defined features driving the rigid foams' structural performance, including stress-strain and failure behaviors, temperature dependency, and orientations due to the manufacturing process. These are the minimum requirements to represent the real influence of the production process as well as the foam morphology on the performance in the end-use applications.

A further criterion for the model, used in the selection of the technical approach to foam modeling, is the ability to represent the material failure in an implicit finite element analysis. In reality, failures of PUR/PIR foams in the aforementioned applications occur over several hours to several days. Moreover, the foam failure is due to differential thermal dilation of the materials considered in end-use applications such as PIR foam core and steel faces. Therefore, only implicit numerical techniques can be used to represent this phenomenon. On the contrary, numerical techniques for modeling crack initiation and propagation pertain to explicit numerical solvers tailored for simulating fast and explosive events like crash tests and air-bag opening. In short, the constitutive model requirements are:

- Ability to depict orientation in stress-strain and failure behavior as well as their dependence upon temperature, and
- Adaptability to implicit analysis.

Based on the criteria above, the Double-Inclusion mean-field homogenization technique developed by Nemat-Nasser and Hori [2] was selected. The Double-Inclusion homogenization technique is implemented in the commercial software Digimat [3], and it is seamlessly integrated with the Abaqus [4] finite element software used for the thermo-mechanical simulation of the PUR/PIR foam-based products. In addition, the Double-Inclusion method was selected because it can consider high inclusions' volume fraction. This is due to the fact that rigid PUR/PIR foams exhibit closed-cell microstructure with a volume fraction of voids or porosity up to 95 %.

The Double-Inclusion homogenization technique was developed for heterogeneous materials consisting of two or more constituents. Therefore, the model requires describing the constituents of the material under study in terms of structural and thermal behavior: Young's modulus as a function of temperature $E(T)$, Poisson's ratio ν, density ρ, and coefficient of linear thermal expansion CLTE(T). In this work, the proposed method, inspired by Gibson and Ashby [5], considers the rigid foam as a composite with two constituents: gas in the cells (i.e., voids) and the

enclosing cell walls structure (i.e., matrix). Figure 5 illustrates the two-constituent composite concept of the PUR/PIR rigid foams in this study. First, the structural behavior of the void phase (Young's modulus E and Poisson's ratio ν) as well as the general orientation of the foam are defined. Then, the matrix morphology and structural behavior can be identified. In particular, the PUR/PIR matrix material elastic behavior, i.e., Young's modulus E and Poisson's ratio ν, as well as morphology, i.e., cell aspect ratio AR, are identified by reverse engineering capability provided by the Digimat-MX module. Digimat-MX provides a "Reverse engineering and parameter identification" tool to optimize and obtain the set of material parameters for the matrix, which minimizes the error between the experimental and numerical tensile stress-strain curves.

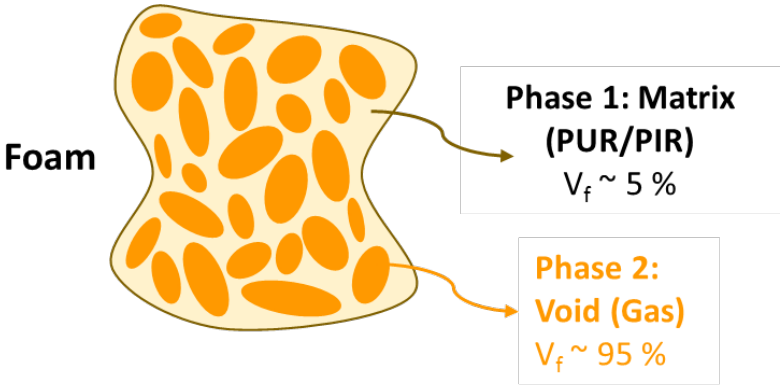


Figure 5. Double-Inclusion homogenization model's schematic for PUR/PIR foams.

3.2 Failure criterion

The failure behavior of the PUR/PIR foams is defined using the Tsai-Wu 3D transversally isotropic failure criterion [6]:

$$f_i = \sqrt{\mathcal{F}_i(\boldsymbol{\varepsilon})}\ with:$$
$$\mathcal{F}_i(\boldsymbol{\varepsilon}) = \frac{\varepsilon_{11}^2}{X_t X_c} + \frac{\varepsilon_{22}^2 + \varepsilon_{33}^2}{Y_t Y_c} + \frac{(2\varepsilon_{12})^2 + (2\varepsilon_{13})^2}{S^2} + \frac{(2\varepsilon_{23})^2}{Y_t Y_c} - \frac{\varepsilon_{11}\varepsilon_{22} + \varepsilon_{11}\varepsilon_{33}}{2X_t X_c} - \frac{2\varepsilon_{22}\varepsilon_{33}}{Y_t Y_c} + \left(\frac{1}{X_t} - \frac{1}{X_c}\right)\varepsilon_{11} + \left(\frac{1}{Y_t} - \frac{1}{Y_c}\right)(\varepsilon_{22} + \varepsilon_{33}) \quad [1]$$

where failure initiation occurs when $f_i = 1$. This failure criterion exhibits five different allowable values, as demonstrated in Figure 6:

- longitudinal tension X_t and compression X_c (direction 1 in Figure 6 or Advance in Figure 3(b))
- transverse tension Y_t and compression Y_c (directions 2 and 3 in Figure 6 or Thickness and Width in Figure 3(b))
- transverse shear S.

Therefore, the model allows for capturing different failure modes, i.e., tension vs. compression vs. shear, as well as failure behaviors in different directions, e.g., along vs. normal to the axis of cell orientation. The Tsai-Wu 3D transversally isotropic failure criteria (equation [1] and Figure 6) for the PUR/PIR foams modeled in this work are calibrated using data from tension, compression and

four-point bending tests performed at 23 ºC and 85 ºC in the advance (longitudinal) as well as width and thickness (transverse) directions.

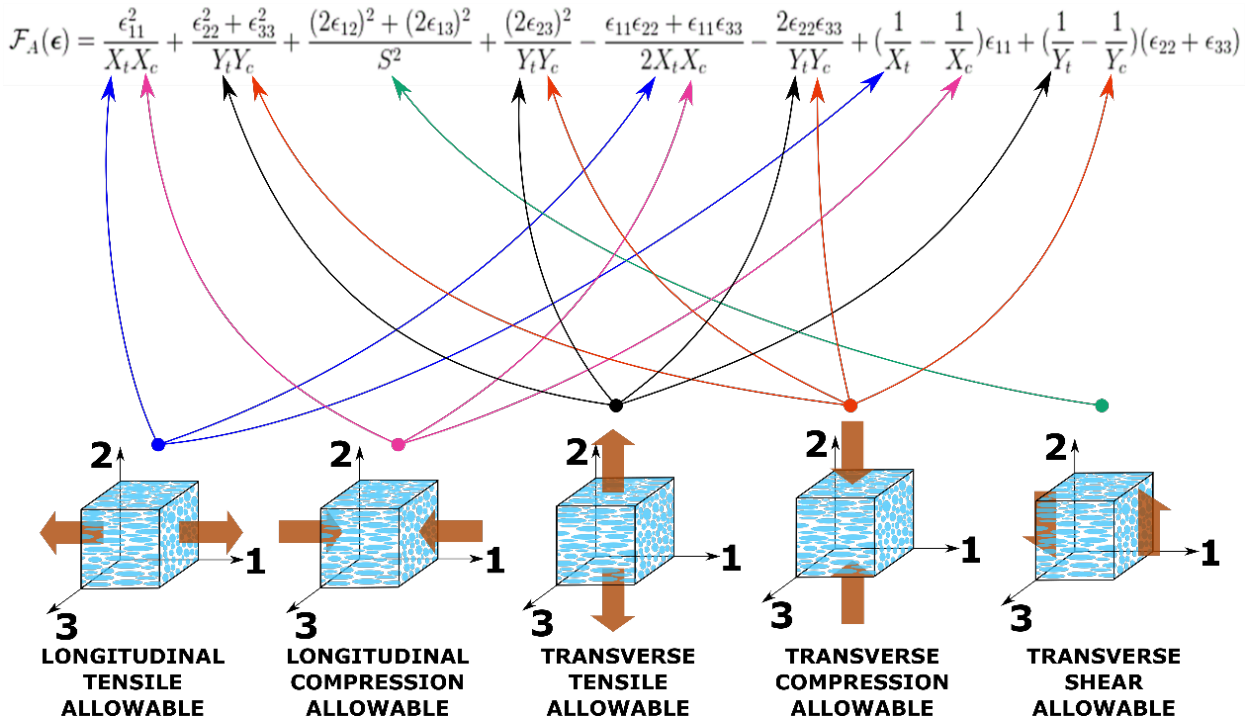


Figure 6. Tsai-Wu 3D Transversally Isotropic failure criterion allowable values.

Once the failure initiation is reached, a linear damage evolution law is used.

$$\acute{\sigma}_0 = (1 - D)\sigma_0$$
$$D = \frac{D_{max}}{\delta\varepsilon_{lim}}\delta\varepsilon \text{ with } \delta\varepsilon_{lim} = \varepsilon - \varepsilon_{ini} \quad [2]$$

Where $\acute{\sigma}_0$ is the stiffness of the damaged material, D is the linear stiffness degradation law, D_{max} is the maximum damage at failure, ε_{ini} is the strain at damage initiation, $\delta\varepsilon_{lim}$ is the change in the strain at which the failure is completely developed.

3.3 Modeling Workflow

The workflow of the proposed modeling approach for rigid foams is demonstrated in detail in Figure 7. Multiple steps are undertaken beginning with the tension, compression, and shear characterization of the foams in the advance, width, thickness directions, and performed at room (23 ºC) and elevated (85 ºC) temperatures. Then, different modules within the Digimat framework are used to calibrate the thermal-mechanical material models based on the experimental data input. Here, the microstructure and orientation dependence of the foam is taken into account via mean-field homogenization. The temperature-dependent thermal-mechanical properties of the foams are also accounted for. The material models are then used in the commercial FEA software Abaqus to evaluate the thermal-structural performance of the end-use applications.

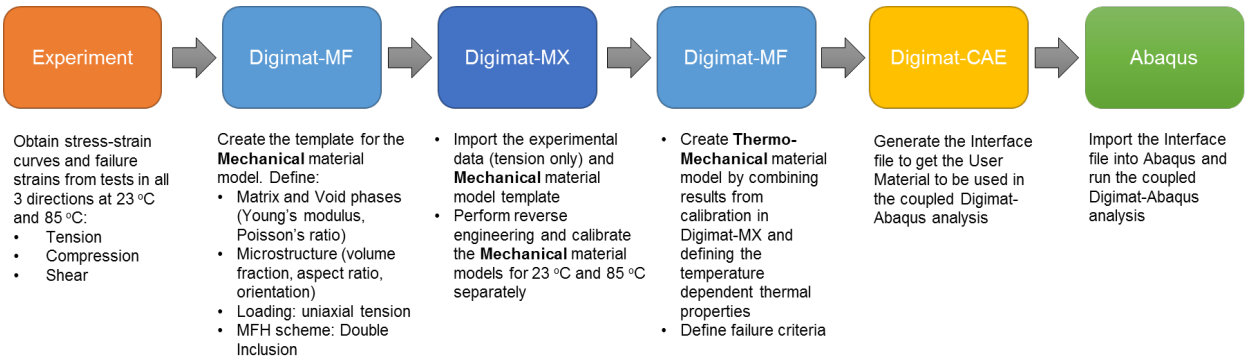


Figure 7. Workflow of the proposed modeling approach.

3.4 Applications

Using the approach and workflow discussed above, the material models for the foams were calibrated in Digimat, then used in macroscale FE models in Abaqus to simulate the tensile and four-point bending tests. The model geometries were created so that they match the validation experiments, which will be discussed in detail in the next section. The model setups are shown in Figure 8. It should be noted that the tensile test model was performed for both 23 ºC and 85 ºC, and the loading directions are parallel to the advance as well as the width and thickness directions of the foams. For the four-point bending tests, the length, width, thickness directions of the specimens correspond to the advance, width, thickness directions of the metal-faced panels.

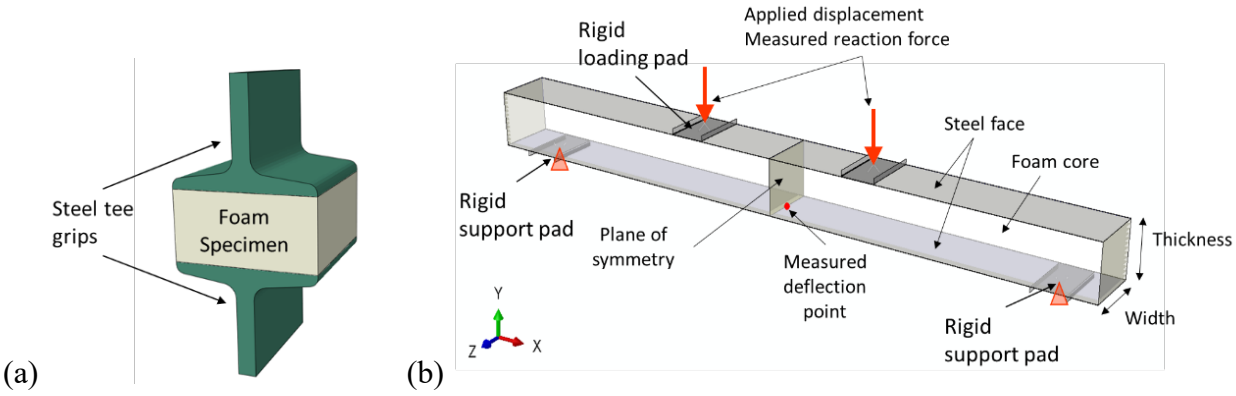


Figure 8. (a) Tensile test model setup (b) Four-point bending test model setup.

4. VALIDATION EXPERIMENTS

4.1 Tensile Tests with Digital Image Correlation

Tensile tests were conducted at 23 ºC and 85 ºC. Foam specimens of dimensions 50 mm x 50 mm x 25 mm were cut from the panel so that the 25-mm dimension is parallel to the advance, width, thickness direction of the panel. Each specimen was adhesively bonded to a pair of steel tee grips. The steel tee grips have dimensions of 50 mm (length) x 50 mm (width) x 50 mm (height) x 6.35 mm (flange thickness). The grips underwent a surface treatment process prior to bonding to ensure proper adhesion between the grips and foam. An Instron frame model 3365 with a 5 kN load cell

and pneumatic loading grips were used. All specimens were loaded in tension at a rate of 1.3 mm/min. Figure 9(a) shows the tensile test setup conducted in this work. The tensile stress-strain responses, as well as modes of failure, were compared to the model's results. In-situ digital image correlation was conducted at room temperature to measure the displacement and strain fields on the foam during loading. Two PointGrey cameras were used to obtain the 3D-DIC measurements. Prior to testing with DIC, the front surfaces of the bonded foam specimen assemblies were spray-coated with black paint to create speckle patterns for the DIC analysis. Poisson's ratios on the foam samples were calculated using the strain fields from the DIC analysis and compared to the model predictions.

4.2 Four-point Bending Tests with Digital Image Correlation

Four-point bending tests were conducted at room temperature, according to European Norm EN 14509 [1] recommendations. The specimens have nominal thickness, width, and length dimensions of 100 mm, 100 mm, and 1050 mm, respectively. The loading and support spans are respectively 300 mm and 900 mm. The width and thickness of the steel loading plates are 100 mm and 10 mm. The tests were performed using an Instron frame model 3365 with a 5 kN load cell and at a loading rate of 12 mm/min. In-situ DIC measurements were conducted to obtain the full-field strain distribution on the foam during loading and at failure. The four-point bending test setup is shown in Figure 9(b).

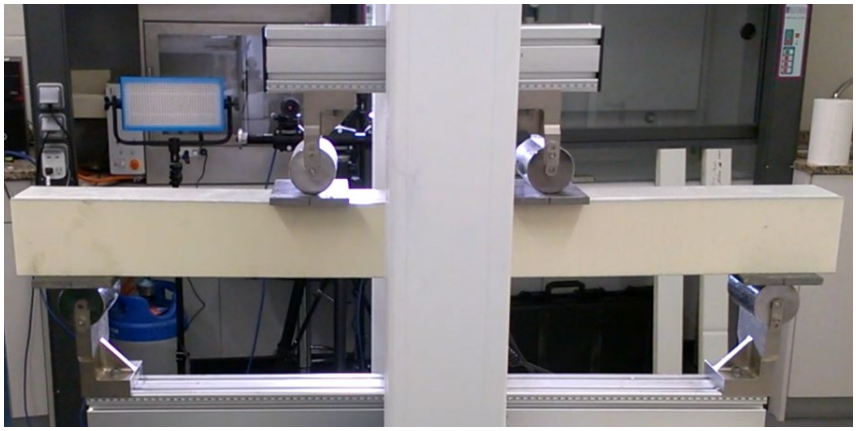
(a)  (b) 

Figure 9. (a) Tensile test setup (b) Four-point bending test setup.

5. RESULTS

It should be noted that the proposed modeling of approach works for rigid foams in general. For this paper, we selected a PIR foam to demonstrate the results of the models and validation experiments.

5.1 Tensile Stress-Strain Responses

Figure 10 shows the comparison between experimental and numerical tensile stress-strain responses in the advance and average of thickness and width directions at 23°C and 85°C of PIR foam. It can be seen that the proposed model represents the tensile behavior of the PIR foam with a high degree of accuracy in terms of stiffness response. Particularly, it captures the foam's higher

stiffness in the advance direction compared to that of the width and thickness directions. In addition, the model is able to represent the relevant variation with temperature of the foam failure behavior at different temperatures. In summary, the proposed Double-Inclusion constitutive model for rigid PUR/PIR foams can accurately represent the thermo-structural behavior of the PIR foam, encompassing orientation, failure, and dependence upon temperature.

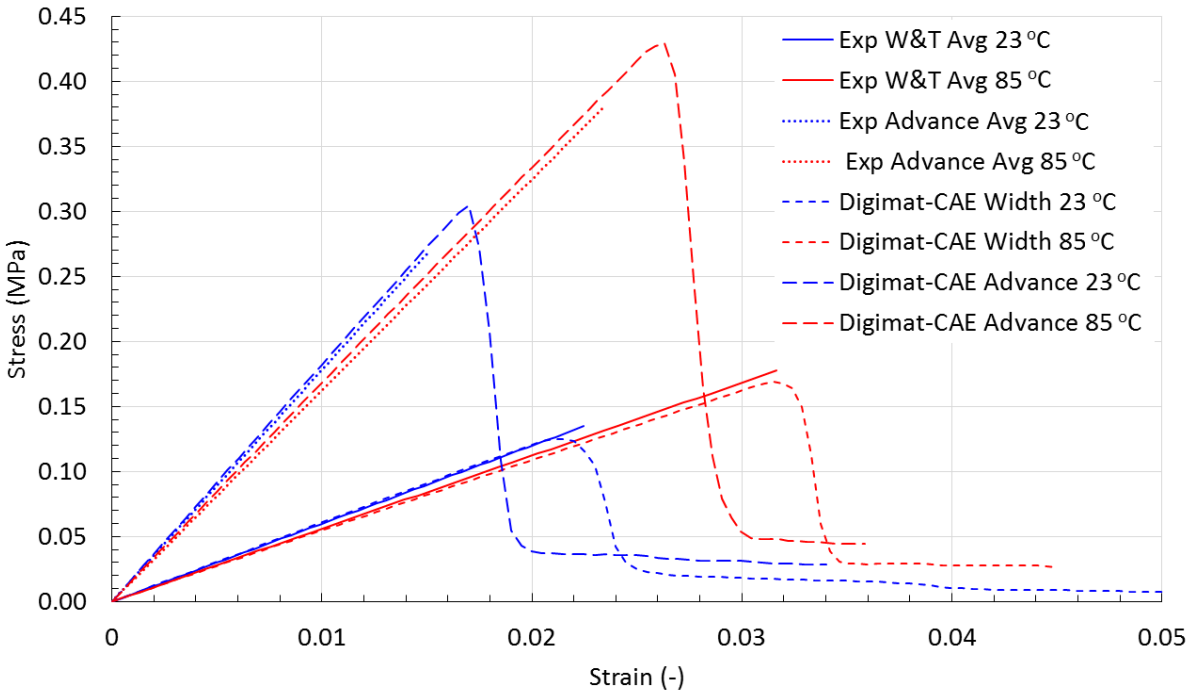


Figure 10. Experimental vs. Numerical: Tensile stress-strain responses in the advance and average of thickness and width directions at 23°C and 85°C of PIR foam.

5.2 Failure Modes and Failure Envelopes

The failure modes of the tensile specimens observed in the experiment and obtained from modeling are shown in Figure 11. The model predicted that failures occur inside the foam near both the top and bottom surfaces of the foam specimen, where it is bonded to the steel tee grips. This corresponds to the high strain levels in the specimen near the grips, as seen in the maximum principal strain contour plots in Figure 11. In reality, each specimen has only one major crack that spans the entire cross-section and locates close to either the top or bottom metal grip. This is because of the random distribution of defects and their sizes inside the foam specimen, and the first defect that causes failure initiation in the locations experiencing high strain will propagate leading to final failure.

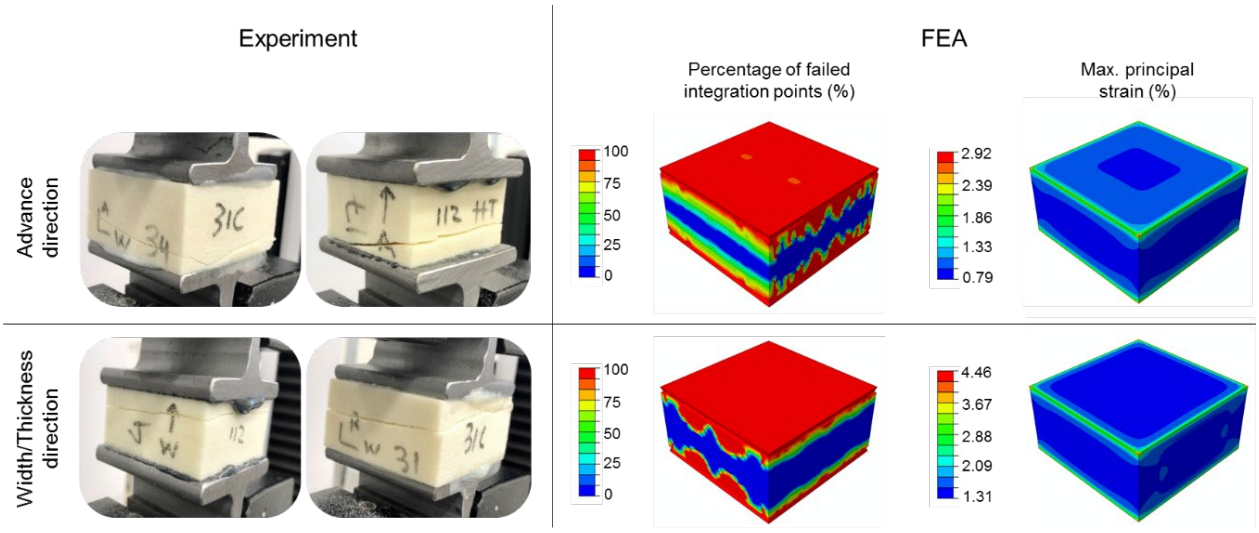


Figure 11. Experimental vs. Numerical prediction: Failure modes.

Table 1 summarizes the allowable parameters obtained from calibration and validation for the Tsai-Wu failure criteria of PIR foam. The identified allowable values in Table 1 reflect the behavior of the foam in different failure modes. PIR foam tends to fail more prematurely in tension than in compression or shear, which is reflected by the X_c, Y_c, S being noticeably higher than X_t and Y_t. This failure behavior is exemplified by the failure envelopes at different temperatures shown in Figure 12.

Table 1. Allowables for the Tsai-Wu failure criterion of PIR foam.

Mode	**Symbol**	**Temperature**	
		23 °C	**85 °C**
Tension	Xt	0.016	0.023
	Yt	0.022	0.032
Compression	Xc	0.065	0.090
	Yc	0.095	0.120
Shear	S	0.075	0.100

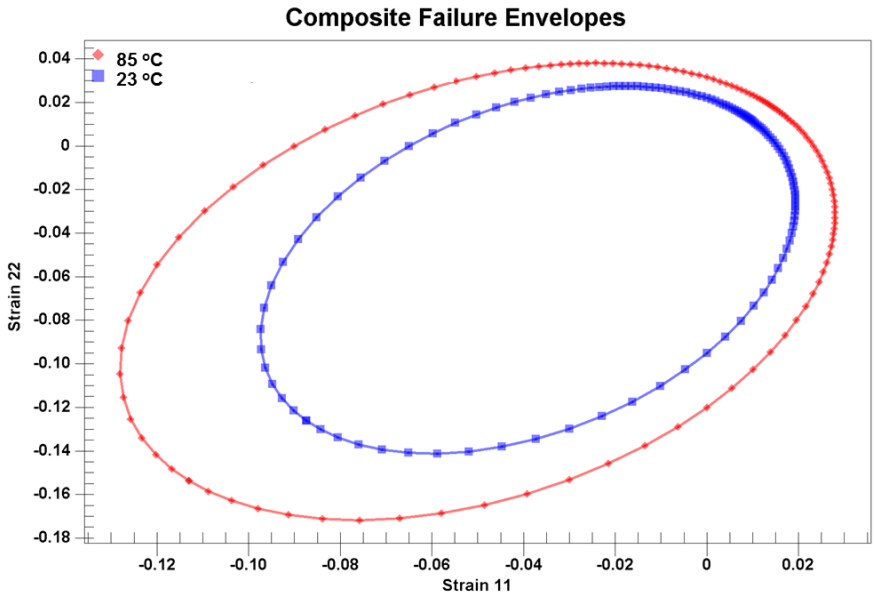


Figure 12. Failure envelopes projected on the $\{\boldsymbol{\varepsilon_{11}} \equiv \boldsymbol{\varepsilon_{Advance}}, \boldsymbol{\varepsilon_{22}} \equiv \boldsymbol{\varepsilon_{W\&T}}\}$ plane.

5.3 Poisson's Ratio

DIC strain measurements were used to calculate and construct full-field distributions of Poisson's ratios. Six different Poisson's ratios were measured and compared to the model predictions. Examples of Poisson's ratios ν_{21} and ν_{23} maps are presented in Figure 13. Figure 14 shows comparisons of the average ν_{21} and ν_{23} measured via digital image correlation and numerical values computed using the Double-Inclusion homogenization method, highlighting the excellent agreement between the predicted and measured Poisson's ratios.

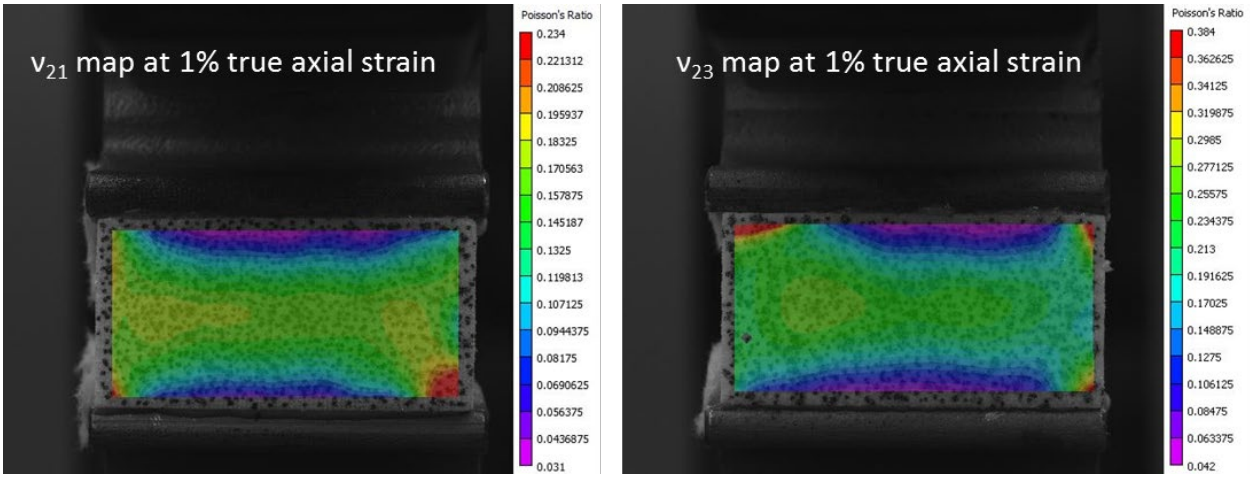


Figure 13. Examples of Poisson's ratio distributions on PIR foam during tensile loading.

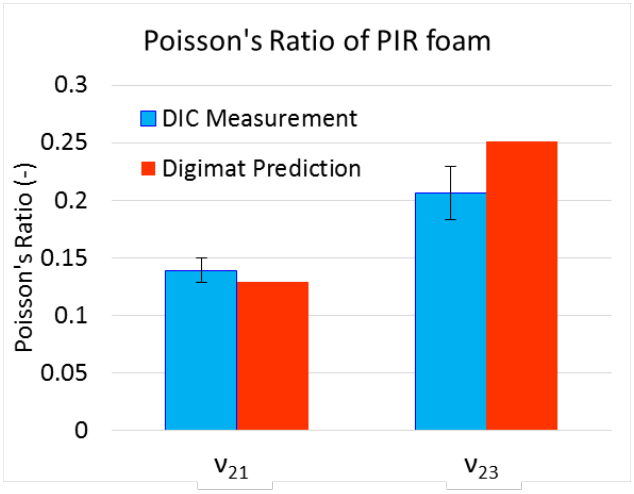


Figure 14. Comparison between model predictions and DIC measurements of PIR foam's Poisson's ratios.

5.4 Four-point Bending Measurements

The load-displacement curves obtained from the four-point bending experiment and numerical model are shown in Figure 15(a). The experimental load-displacement curve is non-linear. The model response is, however, linear until failure. This is because the PIR material model calibrated using the MFH approach in this work assumes the linear-elastic behavior of the foam. The stiffness and strain at failure values from the experiment and numerical model are in good agreement. Figure 15(b) shows the agreement between failure initiations predicted by the FE model and captured in the experiment. The predicted location and initial shape of the shear failure, highlighted by the red dashed boxes in Figure 15(b), are accurate considering the implicit solver used in this work.

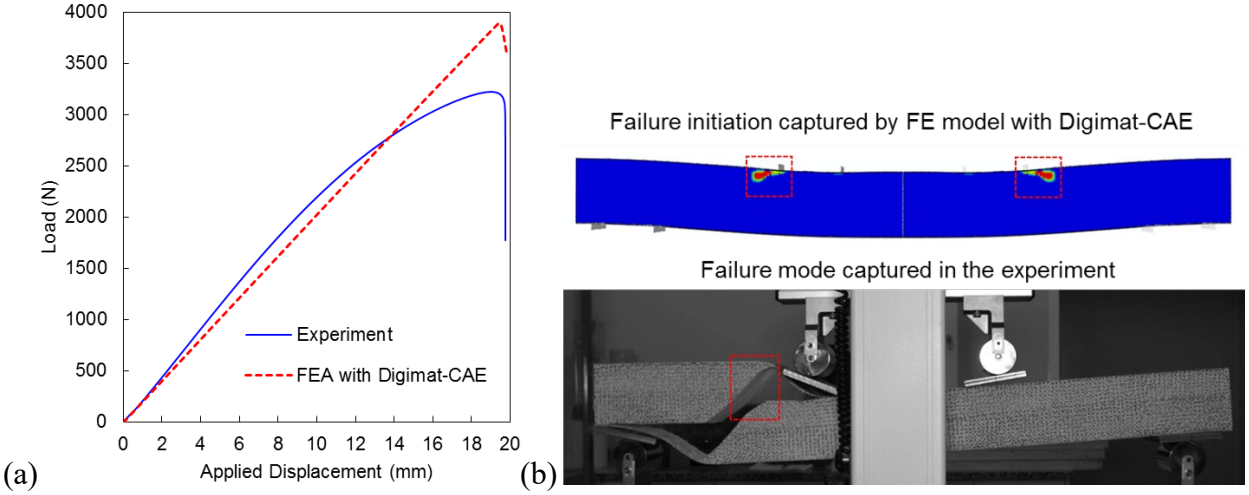


Figure 15. (a) Experimental and numerical comparison of load-displacement curves (b) Failure initiation predicted by the FE model and failure mode captured in the four-point bending experiment.

Full-field distributions of shear and compression strains on the foam obtained from FEA and DIC were compared, as shown in Figure 16. It can be seen that the model predictions are in good agreement with the experimental results. In the shear strain maps in Figure 16(a), the location of maximum shear strain corresponds to the location of failure initiation seen previously in Figure **15**(b). During loading, the foam experience some level of compression. This is captured in both the model and the experiment (Figure 16(b)).

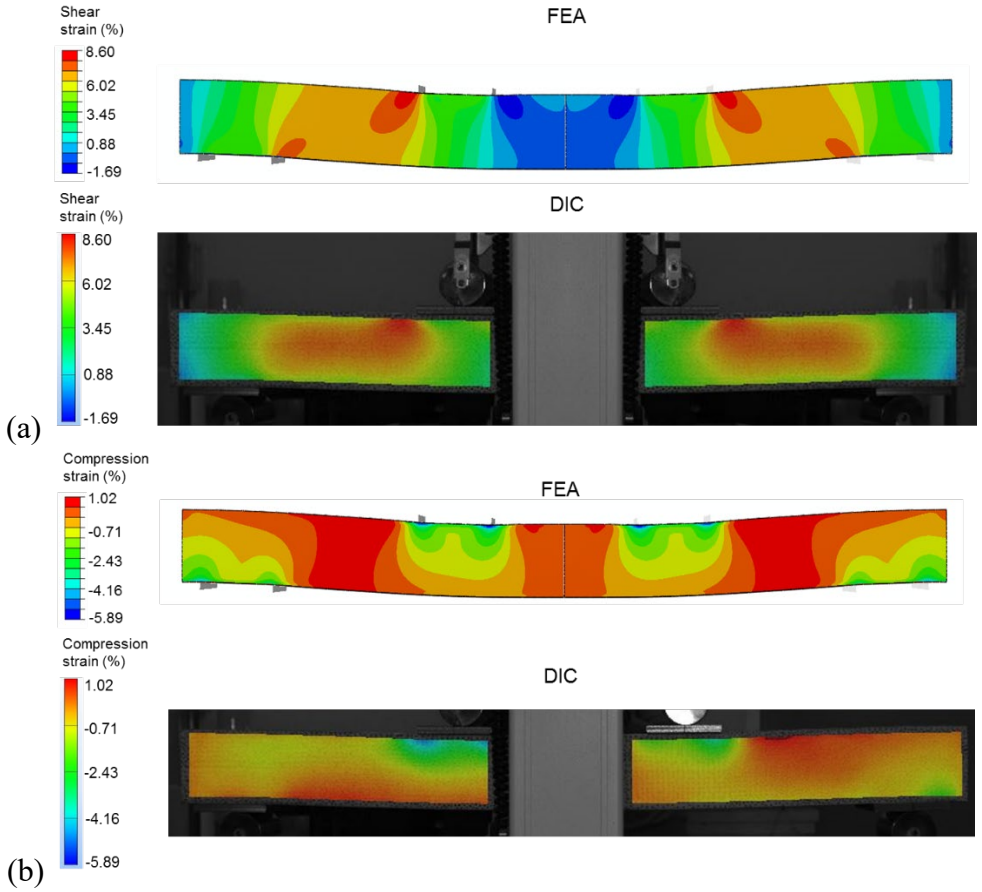


Figure 16. FEA vs. DIC: (a) full-field shear strain before failure (b) full-field compression strain before failure.

6. CONCLUSIONS

In conclusion, this study illustrates a modeling approach, based on the "Double-Inclusion" mean-field homogenization method, proposed by Nemat-Nasser and Hori [2], for modeling rigid PUR/PIR foams encompassing:

- Material orientation due to production;
- Failure;
- Temperature dependence of stiffness and failure.

The proposed approach is suitable for both explicit and implicit solver within Abaqus, allowing one to address fast and explosive events (i.e., crash tests, air-bag opening) as well as slow developing phenomena (i.e., post-production crack creation and propagation due to thermal differential deformation). This approach can be used to evaluate the thermo-structural behavior of

PUR/PIR rigid foams in end-use products such as metal-faced sandwich panels for construction applications.

The proposed model has been successfully validated by means of digital image correlation, direct comparison with tensile tests as well as four-point testing of metal-faced sandwich panels. The model was able to predict with high accuracy the Poisson's ratios of a PIR foam that were measured using digital image correlation. The model for the PIR foam was further validated by comparing numerical and experimental tensile stress-strain data. In addition, the model is able to capture the PIR foam orientation in terms of stiffness as well as failure behavior. Moreover, the effect of temperature variation was represented correctly.

7. REFERENCES

[1] European Norm BS EN 14509:2013, "Self-supporting double skin metal faced insulating panels - Factory made products – Specifications." European Committee for Standardization, 2013.

[2] Nemat-Nasser, S., and Hori, M. *Micromechanics: Overall Properties of Heterogeneous Materials*. Amsterdam: North-Holland, 1993.

[3] Digimat 2018.1 User's Manual.

[4] Abaqus 2018 User's Manual.

[5] Gibson, L.J, and Ashby, M.F. *Cellular Solids: Structure and Properties*. Cambridge: Cambridge University Press, 1997.

[6] Tsai, S.W. and Wu, E.M. "A General Theory of Strength for Anisotropic Materials," *Journal of Composite Materials* 5(1) (1971): 58-80.